THE COMPANY OF
Biologists

RESEARCH ARTICLE

Suction feeding across fish life stages: flow dynamics from larvae to adults and implications for prey capture

Sarit Yaniv[1,2], David Elad[3] and Roi Holzman[4,*]

ABSTRACT

Suction feeding is thought to be the primary mode of prey capture in most larval fishes. Similar to adult suction feeders, larvae swim towards their prey while rapidly expanding their mouth cavity to generate an inward flow of water that draws the prey into the mouth. Although larvae are known to experience flows with lower Reynolds numbers than adults, it is unclear how the suction-induced flow field changes throughout ontogeny, and how such changes relate to prey capture performance. To address these questions, we determined mouth dimensions and opening speeds in *Sparus aurata* from first-feeding larvae to adults. We proceeded to develop a computational model of mouth expansion in order to analyze the scaling of suction flows under the observed parameters. Larval fish produced suction flows that were around two orders of magnitude slower than those of adults. Compared with adult fish, in which flow speed decays steeply with distance in front of the mouth, flow speed decayed more gradually in larval fish. This difference indicates that viscous forces in low Reynolds number flows modify the spatial distribution flow speed in front of the mouth. Consequently, simulated predator–prey encounters showed that larval fish could capture inert prey from a greater distance compared with adults. However, if prey attempted to escape then larval fish performed poorly: simulations inferred capture success in only weakly escaping prey immediately in front of the mouth. These ontogenetic changes in Reynolds number, suction-induced flow field and feeding performance could explain a widespread ontogenetic diet shift from passive prey at early life stages to evasive prey as larvae mature.

KEY WORDS: CFD, Critical period, Laminar flow, Larval fish, Reynolds numbers

INTRODUCTION

The larval stage of most marine fish is spent in the pelagic environment, where they suffer very high mortality rates as a result of predation, advection away from favorable habitats and starvation (Cowen, 2002; Hunter, 1980; Leis and McCormick, 2002). Newly hatched larvae subsist on a limited supply of yolk and must therefore capture food before their energy resources become depleted (Fyhn, 1989; Hunter, 1981). The success rate of prey capture by larval fish rapidly increases with age (Houde and Schekter, 1980; Hunter, 1981). As larvae mature, their skeleton gradually ossifies, body and mouth grow and they experience a hydrodynamic regime

characterized by higher Reynolds numbers (Hernández, 2000; Houde and Schekter, 1980; Müller and van Leeuwen, 2004; Osse and van den Boogaart, 1999; Osse, 1989). These changes improve larval swimming and c-start performance, as well as detection of prey (Danos and Lauder, 2012; Müller et al., 2008; Müller and van Leeuwen, 2004; Müller and Videler, 1996; Osse and van den Boogaart, 1999). It has also been hypothesized that the hydrodynamic regime experienced by small larvae reduces their encounter rates with prey or limits their ability to capture prey (Anto and Turingan, 2010; China and Holzman, 2014; Hernández, 2000; Houde and Schekter, 1980; Osse, 1989).

It is widely accepted that many larval fishes capture their prey using suction and that the biomechanics of larval suction feeding is similar to those of adult fish (Hernández, 2000): both expand the oral cavity in order to drive a volume of water containing the prey into the mouth. The ingested volume of water, distance between mouth and prey and flow speed are important variables contributing to the ability of the predator to overcome the predator-avoidance tactics of the prey and draw it into the mouth (Holzman et al., 2007; Wainwright and Day, 2007).

The hydrodynamics of prey capture in adult and juvenile fish are well characterized (Day et al., 2005; Higham et al., 2006; Holzman et al., 2008a; Müller et al., 1982; Staab et al., 2012; Van Wassenbergh and Aerts, 2009). In bluegill sunfish, flow visualization of suction flows in an ontogenetic series of young-to-adult with peak gape diameter (defined as the maximal diameter of the mouth aperture) of 3–15 mm demonstrated stronger flows in the larger fish (Holzman et al., 2008a). Additionally, larger fish drew water from a greater absolute distance compared with juveniles and flow speed could be estimated from the rate of volumetric expansion of the mouth cavity and gape diameter (Holzman et al., 2008a). Flow visualization revealed flow patterns outside the mouth that conform to the prediction of analytical models (Müller et al., 1982). Flow speeds were symmetrical around the central axis of the mouth and, regardless of gape diameter, speed decayed steeply from its maximum at the mouth center to <10% of the maximum at a distance of one gape diameter away (Day et al., 2005; Higham et al., 2006; Holzman et al., 2008a; Müller et al., 1982; Staab et al., 2012; Van Wassenbergh and Aerts, 2009).

In contrast to adult and juvenile fish, the hydrodynamics of suction feeding in larvae is less clear. Larval fish operate in low Reynolds numbers (*Re*), where viscosity effects are greater, and the equations describing fluid flow are nonlinear (Tuck, 1970). A two-dimensional Navier–Stokes model of a carp larva revealed a strong dependency of suction flows on the fluid viscosity (Drost et al., 1988). In a simulated larval feeding at $Re \approx 150$, about 40% of the energy spent on mouth expansion was lost to frictional forces rather than to accelerating water towards the mouth. Dynamic scaling experiments, in which *Sparus aurata* Linnaeus 1758 (gilt-head seabream) larvae were immersed in solutions up to eight times more viscous than seawater, indicated that the ability of larvae to capture

[1]Department of Zoology, Faculty of Life Sciences, Tel Aviv University, Tel Aviv 69978, Israel. [2]Department of Software Engineering, Afeka College of Engineering, Tel Aviv 69107, Israel. [3]Department of Biomedical Engineering, Faculty of Engineering, Tel Aviv University, Tel Aviv 69978, Israel. [4]The Inter-University Institute for Marine Sciences, POB 469, Eilat 88103, Israel.

*Author for correspondence (holzman@post.tau.ac.il)

The Journal of Experimental Biology

List of symbols and abbreviations

B_1, B_2, B_3	lengths of the lateral surfaces of each compartment of the mouth
L	length of the mouth cavity (mm)
L_1, L_2, L_3	length of each of the three mouth sections (mm)
R	Euclidean distance from the longitudinal axis to a point P (unit length of peak gape diameters)
$R_1(t), R_2(t), R_3(t)$	time-dependent radius of each mouth section, at the anterior end of the section (mm)
$R_{1,max}$	maximal radius of the mouth aperture (mm)
t	time (s)
$U(t)$	flow speed at time t (m s^{-1})
U_m	flow speed at the center of the mouth aperture ($R,Z = 0,0$) (m s^{-1})
$U_{m,max}$	maximal flow speed at the center of the mouth aperture ($R,Z = 0,0$) (m s^{-1})
Z	signed distance from the plane of the mouth to point P (unit length of peak gape diameters)
$v(t)$	flow speed at time t in units of $U_{m,max}$

---

prey is largely determined by the Re regime in which they feed (China and Holzman, 2014). Nevertheless, the existing models have not quantitatively compared the spatial flow fields in larval fish with those of adults, despite the potential impact of lower Re regimes on prey-capture performance in first-feeding larval fish.

The ability of a predator to capture its prey using suction flows can be described by the ratio of suction forces generated by the predator to the body mass of the prey (Wainwright and Day, 2007). This framework can provide a useful tool to understand how variations in predator and prey traits affect feeding success. In adult fish, the forces exerted on the prey depend on multiple predator traits such as peak gape diameter, mouth opening speed and the velocity of jaw protrusion (Holzman et al., 2012). Moreover, different prey types impose different demands for their capture and predator traits that were shown to be important for capture of evasive prey were less important for attached prey (Holzman et al., 2012). Because prey types commonly change during fish ontogeny, some functional traits may become more or less important as the fish

transition from larva to juvenile to adult. For example, in adult fish, the hydrodynamic force exerted on a prey is dominated by the pressure gradient across the body of the prey. Generation of steep pressure gradients generally depends on the ability of the fish to induce fast suction flows with high accelerations, which are usually associated with larger fish (Holzman et al., 2008b; Holzman et al., 2007; Wainwright et al., 2007; Wainwright and Day, 2007). However, previous studies also suggested that smaller gape diameters produce steeper flow-speed gradients, which increase the forces experienced by the prey (Skorczewski et al., 2010; Wainwright and Day, 2007) and it is unclear how these mechanisms combine to affect prey capture in larval fish.
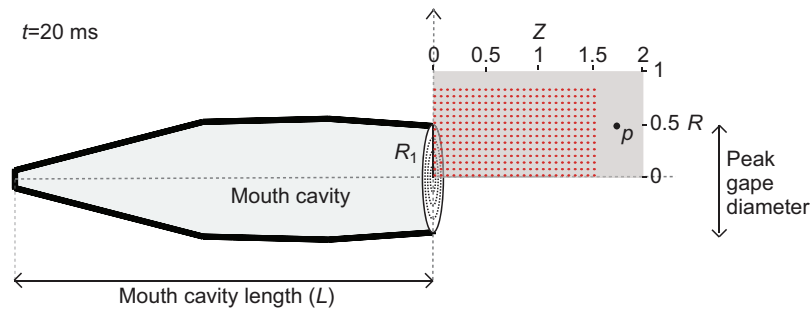
The goals of the present research were: (1) to describe the flow field in front of the mouth in an ontogenetic series of fish from first-feeding larvae to adults; and (2) to assess how changes in flow field affect the capture of both inert and escaping prey. Based on the scaling of mouth dimension and mouth-opening speed in *S. aurata*, we developed a computational model of fluid flow during suction feeding. Mouth cavity was modelled as a series of three interconnected truncated cones, and mouth expansion occurred as a coordinated motion of the three cones. We evaluated the fluid flow patterns in front of the mouth at several life stages, and used these results to assess how changes in the spatial distribution of flow, peak flow speeds and mouth size affect the ability to capture both inert and evasive prey.

RESULTS
Ontogeny of mouth-cavity dimensions and expansion
The growth of peak gape diameter ($2 \times R_{1,max}$; Fig. 1) with respect to mouth cavity length (L) had a slope of 0.95 (±confidence intervals [CI]=0.032; Fig. 1A; linear regression on log-transformed values, $F_{1,35}$=2470; $P<0.001$; R^2=0.98). The time to peak gape (defined as the time it took the fish to open its mouth from 20% to 95% of peak gape diameter; $t_{1,max}$) ranged from 9 to 76 ms (n=47 strikes) and was not correlated with fish standard length, mouth cavity length or peak gape diameter (Fig. 1A; linear regression; $P>0.1$; $R^2<0.1$ for all variables). Quantile regression further showed no relationship
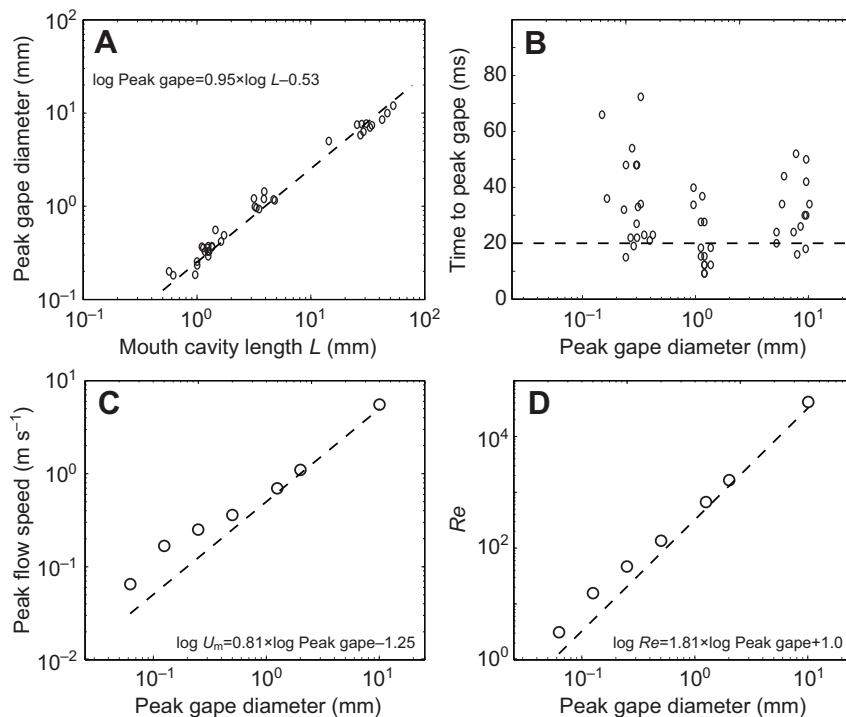
Fig. 1. **Mouth cavity dimensions, expansion, and flow speed in *Sparus aurata*.** (A) Peak gape diameter as a function of mouth cavity length. The dashed line corresponds to the slope from a major axis regression. (B) Time to peak gape as a function of peak gape diameter. The dashed line corresponds to the slope from a quantile regression (lower 25%). (C) Peak flow speed at the center of the mouth aperture ($U_{m,max}$) as a function of peak gape diameter. (D) Maximal Reynolds number (Re) at the center of the mouth aperture as a function of peak gape diameter. Data in A,B are from measurements on *S. aurata*, data from C,D are from the CFD model. The dashed line in C,D corresponds to flow speed and Re expected based on the time-dependent volumetric expansion of the mouth and gape diameter alone.

In plot A: log Peak gape=0.95×log L−0.53

In plot C: log U_m=0.81×log Peak gape−1.25

In plot D: log Re=1.81×log Peak gape+1.0

Fig. 2. Coordinate system used for analysis. We defined a cylindrical coordinate system, with the origin [0,0] at the mouth center and the longitudinal axis set parallel to the mouth center line. In this coordinate system, the radial distance R was the Euclidean distance from the longitudinal axis to the point P and the distance Z was the signed distance from the plane of the mouth to the point P. The unit length of R and Z on the radial and longitudinal axes was defined as one peak gape diameter ($2 \times R_{1,max}$). R_1 was the time-dependent radii of the mouth aperture (Eqn 1, Fig. 9B). In this example, the coordinates of P are $[R,Z]=[0.5,1.75]$. During simulations, flow speed was sampled parallel to the longitudinal axis at radial distances of $R=0$, 1/8, 1/4, 3/8 and 1/2. Inert particles (red dots) were seeded with a homogenous density distribution outside the mouth (supplementary material Table S1, Fig. S1). Note that the arrangement of particles is depicted at $t=0$ ms, whereas the mouth shape shown is for $t=20$ ms.

between peak gape diameter and the time to peak gape in the fastest 25% of sampled strikes (estimated slope ± CI=0.73±1.05) and that the estimated intercept (mean time to peak gape diameter in the fastest strikes) was 19.7 ms (lower and upper CI=9.1 and 1.5, respectively).

Scaling of flow speed

The flow pattern in front of the mouth was analyzed using a cylindrical coordinate system, with the origin at the mouth aperture center and the longitudinal axis along the mouth center line (Fig. 2). In this coordinate system, a point (P) can be described by its radial distance (R=the Euclidean distance from the longitudinal axis) and its longitudinal distance (Z=the signed distance from the plane of the mouth to the projection of P onto the longitudinal axis). The unit lengths R and Z on the radial and longitudinal axes were scaled to peak gape diameter ($2 \times R_{1,max}$).

Flow speeds were strongly dependent on mouth cavity dimensions and expansion speeds. At the center of the mouth aperture $[(R,Z)=(0,0)]$, maximal flow speed $U_{m,max}$ was higher for mouths with larger gape diameters (Fig. 1C). The rate of increasing flow speed with increasing peak gape diameter was faster for mouths with peak gape diameters >0.5 mm. Reynolds numbers were also higher for mouths with peak gape diameters >0.5 mm because of the concomitant increase in maximal flow speed (Fig. 1D). The

model with the largest peak gape diameter (10 mm) was characterized by a maximal $Re \approx 10^4$, whereas models with the smallest gape diameter (<0.5 mm) were well below maximal Re of 10^2.

The time of peak flow speed {defined as the time of maximal flow speed at the center of the mouth aperture $[(R,Z)=(0,0)]$} coincided with the peak of the first derivative of mouth cavity volume displacement with respect to time. For mouths with peak gape diameters <0.125 mm, peak flow speed occurred at $t=8.5$ ms, whereas for the largest diameter, peak flow speed occurred at $t=10$ ms. Nonetheless, no significant relationship was observed between peak gape diameter and the time of peak flow speed ($r<0.2$, $P>0.1$).

To compare the spatial pattern of suction flows across mouths in which peak gape diameters and peak flow speed spanned two orders of magnitude, we defined scaled flow speed $\upsilon(t)$ as flow speed at any given point in space divided by peak flow speed at the center of the mouth aperture of each model. This analysis revealed that the pattern of fluid velocity in front of the mouth changed with peak gape diameter. Fig. 3 illustrates that in models with peak gape diameters of 0.0625 and 0.125 mm, flow speed gradients along the mouth center line (Z-axis) are more gradual, and flows reach a greater scaled distance than in models with peak gape diameters of 1.25 and 10 mm. For large mouths with gape diameters ≥0.5 mm,
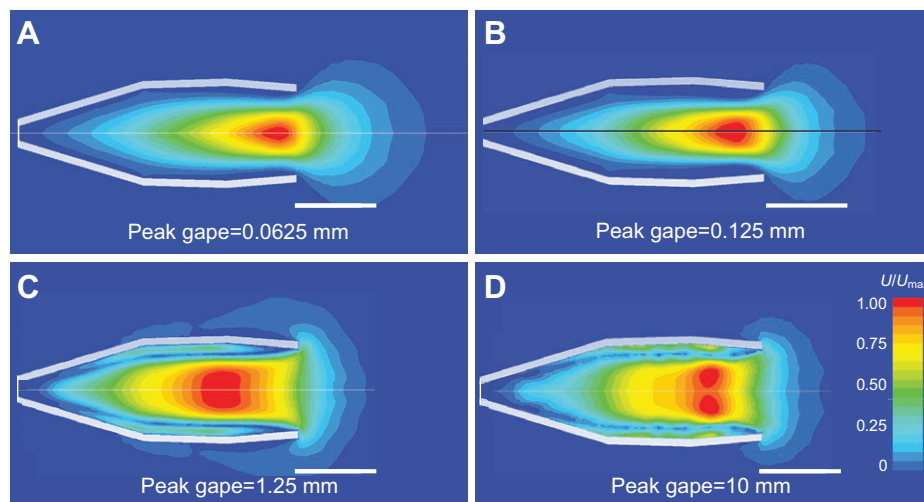
Fig. 3. Flow speed map of suction flow at time of peak mouth expansion. Data are shown for $t=20$ ms for peak gape diameters equal to (A) 0.0625 mm, (B) 0.125 mm, (C) 1.25 mm and (D) 10 mm. The scale bar is equivalent to gape diameter at $t=20$ ms. The speed is proportional to the maximal flow speed across the entire domain. Note that the figure captures only part of the computational domain.
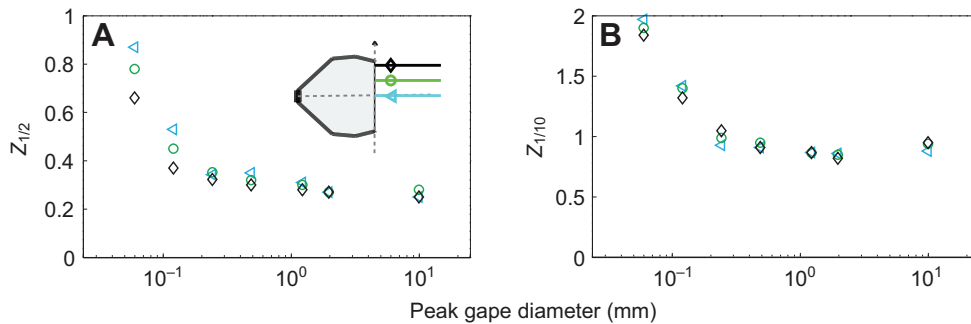
Fig. 4. Decay of flow speed in front of the mouth at t=20 ms. (A) $Z_{1/2}$ is the scaled distances (in units of peak gape diameters), at which flow speed equals half of flow speed at the center of the mouth aperture. (B) Similarly, $Z_{1/10}$ is the scaled distances at which flow speed equals tenth of flow speed at the center of the mouth aperture. Flow speed was extracted parallel to the longitudinal axis at radial distances of R=0, R=0.25 and R=0.5 (blue triangles, green circles and black diamonds, respectively).

scaled flow speed $\upsilon(t)$ decayed by half at Z=0.35 mouth diameters and to 0.10 at Z=1 (Fig. 4). These patterns were also evident from measurements at various radial distances R above the longitudinal axis (Figs 4, 5). Flow speeds were largely uniform over the mouth aperture, except for an area of slow flow near the mouth rim (Fig. 6). For small mouths with peak gape diameters <0.5 mm, $\upsilon(t)$ decayed at a lower rate (Fig. 4). For the smallest mouth (peak gape diameter=0.065 mm), $\upsilon(t)$ decayed by half at Z=0.85 and to 10% at Z=2. For these gape diameters, velocities farthest from the longitudinal axis (R >1/4) decayed more gradually than did those observed on the longitudinal axis (R=0; Fig. 5). In the smallest mouth, a parabolic profile was observed for the flow speed across the mouth aperture (Fig. 6). These results indicate a strong effect of viscous forces at low Reynolds number flows on the spatial distribution of flow speeds in front of the mouth.

Capture of inert particles

The potential of fish to capture inert prey was analyzed from the fate of simulated inert particles that were present in front of the mouth aperture at the onset of the suction flows and were tracked through the simulated mouth opening (Figs 2, 7). For large mouths with peak gape diameter ≥0.5 mm, particles were entrained from Z≤0.9, whereas for smaller mouths with peak gape diameter <0.5 mm particles were entrained from larger distances of up to Z=1.26. In the largest mouth (peak gape diameter=10 mm), 54.1% of the seeded particles in front of the mouth aperture were captured, whereas in the smallest one (with peak gape diameter=0.0625 mm), 77.2% of the particles were entrained.

Capture of evasive prey

The potential to capture escaping prey was determined as the thrust required by simulated prey to evade capture (hereafter 'escape thrust'). Mouths with larger gape diameters (and faster suction flows) required prey to exert higher escape thrust. Furthermore, large mouths with peak gape diameter >0.5 mm could capture prey that started their escape from greater distances of up to Z=0.9 peak gape diameters (Fig. 8). Prey had to exert forces ranging from ~10^{-7} to 10^{-10} N, depending on the initial distance from the mouth, in order to escape these large gape diameters. Small mouths with peak gape diameters ≤0.5 mm could capture escaping prey from only a limited distance. For example, maximal prey capture distance was Z=0.62 for mouth diameter=0.5 mm and Z=0.18 for peak gape diameters of 0.125 mm. Prey had to exert forces ranging from ~10^{-9} to 10^{-12} N, depending on initial distance from the mouth, to escape these small gape diameters. No prey was captured by the mouth with the smallest peak gape diameter (0.0625 mm), even at the closest initial distance of 0.1 gape diameters.

DISCUSSION

On the basis of the observed scaling of mouth dimensions and mouth-opening speed in *S. aurata*, we developed a computational model of mouth expansion and evaluated the fluid flow patterns in front of the mouth at several life stages. Simulations revealed that transition into a regime of Re<100 (peak gape diameter <0.5 mm) strongly affected the characteristics of suction flows. The scaling of peak flow speed with peak gape diameter size showed negative allometry (Fig. 1) and spatial flow speed gradients on the
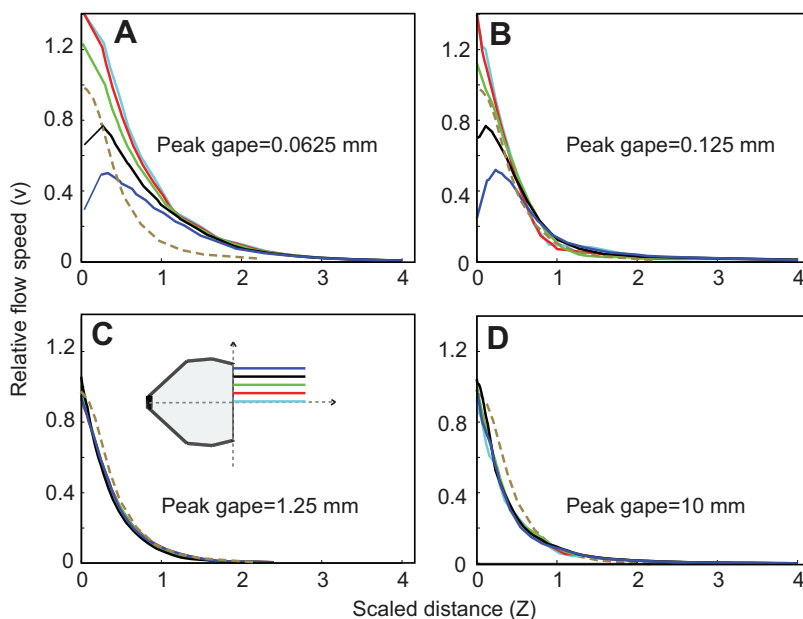
Fig. 5. Representative flow speed profiles at the time of peak gape (t=20 ms). Data are shown for models with peak gape diameter of (A) 0.065 mm, (B) 0.125 mm, (C) 1.25 mm and (D) 10 mm. Flow speed was extracted parallel to the longitudinal axis at radial distances of R=0, 1/8, 1/4, 3/8 and 1/2 (light blue, red, green, black and dark blue lines, respectively). Flow speeds are relative to the flow speed at the center of the mouth aperture. Flow speed profiles derived from the circular vortex model (Müller et al., 1982) are outlined in the dashed brown line.
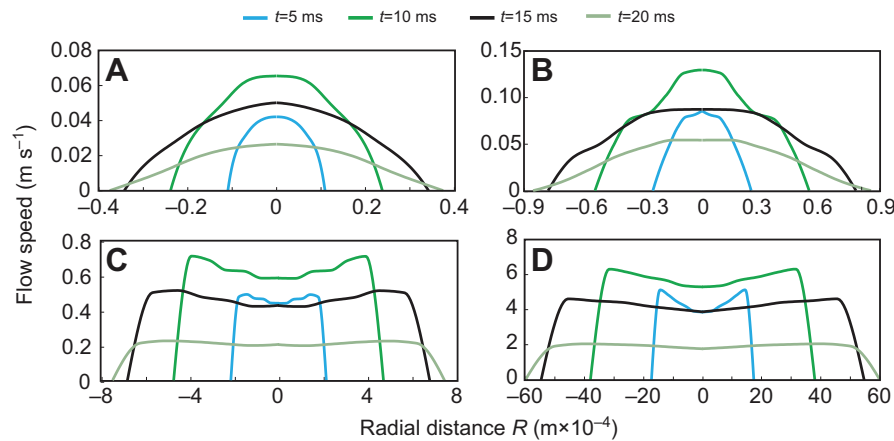
Fig. 6. Representative flow speed profiles across the mouth aperture ($Z=0$). Data are shown for models with peak gape diameter of (A) 0.065 mm, (B) 0.125 mm, (C) 1.25 mm and (D) 10 mm. The *x*-axis represents to the radial distance (on the *R* axis) from the center of the aperture. Data are shown for $t=5$, 10, 15 and 20 ms.

longitudinal axis become less steep at smaller gape diameters (Figs 3–5). For mouths with smaller peak gape diameter, inert prey in front of the mouth were drawn from greater normalized distances than for large gape diameters (Fig. 7). However, the ability of small mouths to capture evasive prey is greatly compromised, as they were only able to capture weakly escaping prey and from a very close strike initiation distance (Fig. 8).

### Implications for larval feeding

Changes in peak flow speed and the spatial distribution of flow that result from increasing mouth size combine to strongly affect scaling of feeding performance. The smallest mouths (e.g. 0.065–0.25 mm) could draw passive prey from the greatest scaled distance (relative to mouth diameter), but their performance dropped dramatically when prey utilized even moderate escape thrusts. Larval fish are therefore more effective in capturing passive prey, which can include the eggs of fish and invertebrates, and particulate organic materials. Indeed, although these prey are frequently captured by fish at all life stages, they make up the overwhelming majority of larval fish diets (Hillgruber et al., 1995; Holzman and Genin, 2003; Kent et al., 2006; Sponaugle et al., 2010).

In contrast, because small mouths can produce only weak suction flows, they are very limited in their ability to capture evasive prey, such as copepods, shrimps, krill and fish (Holzman et al., 2007). The combination of lower flow speed and more moderate flow gradients in larval fish results in weaker pressure gradient forces exerted on the prey. Consequently, larval fish suffer a performance decrement when feeding on prey that employ an escape response, as is illustrated in the negative correlation between maximal capture distance and mouth size for both absolute (Fig. 8A) and scaled (Fig. 8B) distances, and by the negative correlation between maximal escape thrust (at any starting distance) and mouth size.

Our results are consistent with previous observations showing that, for evasive prey, capture distances is greater for larger gape diameter even within the range of mouth sizes exhibited in larval fish. China and Holzman (China and Holzman, 2014) quantified the distance between larval *S. aurata* and their swimming prey at the time of mouth opening. They observed that although young larvae (8 days post hatching) attempted to strike only on prey at a distance of 0.7 mouth diameters from the mouth, their success rate at this close range was negligible. At 13 days post hatching, larvae were successful in capturing prey at a distance of up to 0.8 mouth
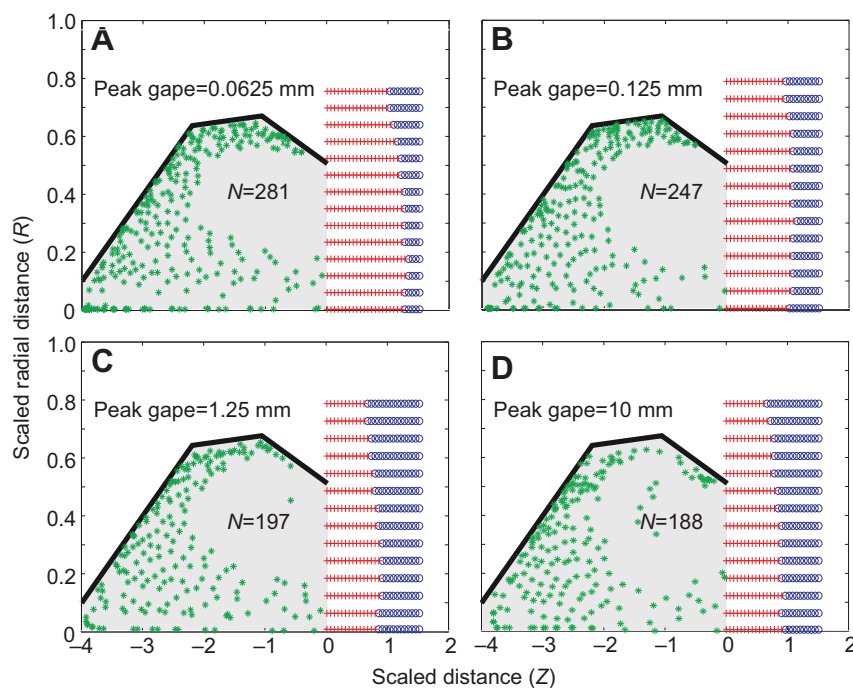
Fig. 7. Capture of inert particles. A total of 364 inert particles were seeded in front of the mouth, with the closest particle located at [R,Z]=[0,0] and the farthest at [0.78,1.5]. Particles were homogenously distributed in this area, with spacing of $R=Z=0.06$ (see Fig. 2; supplementary material Table S1). The fate of the particles at $t=20$ ms was noted; blue circles indicate the initial ($t=0$ ms) locations of particles that were not entrained into the mouth, while red plus signs represent the initial ($t=0$ ms) locations of entrained particles. Asterisks represent the final locations of entrained particles. The number of entrained particles (N) is denoted on each panel. The shaded gray area (black margins) represents the fully expanded mouth ($t=20$ ms). Data are shown for peak gape diameter of (A) 0.0625 mm, (B) 0.125 mm, (C) 1.25 mm and (D) 10 mm. The unit length *R* and *Z* on the radial and longitudinal axes was defined as one peak gape diameter.
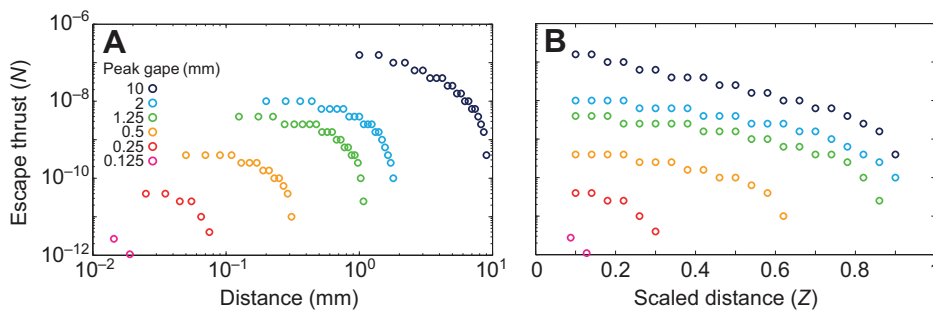
Fig. 8. Escape thrust required for evasive prey to avoid capture. *X*-axis depicts the absolute (A) and scaled (B) strike initiation distance for each simulated strike. Escape thrust was calculated across strike initiation distances of $Z=0.1–1.5$ peak gape diameters. Simulated prey was located on the longitudinal axis ($R=0$). Simulated prey had the same dimensions for all mouth sizes. Data where prey was not captured are not shown.

diameters from the mouth, and larvae at 22 days post hatching captured prey at a distance of up to 1.2 mouth diameters. This increase in prey capture distance corresponded to a fivefold increase in prey capture success (China and Holzman, 2014).

We found that the decay of flow speed in small mouths varies across the mouth opening (Fig. 5). Consequently, small mouths (<0.5 mm) can have low performance for prey that is not located directly in front of the mouth, that is, off the longitudinal axis ($R>0.75$ mouth diameters). We note that our inferences of prey-capture abilities are valid only for prey located in front of the mouth (supplementary material Fig. S1). However, this inference is justified by the observation that fish generally position themselves such that the prey is located in front of the mouth (Drost, 1987; Higham et al., 2006; Kane and Higham, 2014).

Our results provide a plausible mechanistic explanation for the widespread observation that larval fish diets include increasing proportions of evasive prey as the larvae grow. Laboratory experiments with *S. aurata* larvae showed that the proportion of live prey in the diet increased during the first 10 days after feeding commenced, whereas the proportion of inert particles decreased (Fernández-Diaz et al., 1994), despite the constant density of the two prey types. In the wild, individuals of this species shifted to feeding heavily on copepods and mysids as juveniles (Tancioni et al., 2003). This ontogenetic shift in selectivity [the acquisition of a prey type in proportions that differ from its relative density around the predator (Chesson, 1983)] seems to be a common trend in fish. In laboratory experiments, young larval herring fed on poorly escaping mollusk veligers and copepod nauplii in proportions significantly greater than their relative density around the predator, but shifted to more evasive copepods and copepodites at later larval stages (Checkley, 1982). Similarly, Gulf menhaden fed in the laboratory on poorly escaping tintinids and later switched to copepod nauplii (Stoecker and Govoni, 1984). In the wild, Atlantic cod larvae shifted their diet from poorly escaping copepod nauplii at early stages to copepod females that exhibited strong escape responses (Robert et al., 2011). Similarly, first-feeding larvae of walleye pollock fed exclusively on copepod nauplii and copepod eggs (Hillgruber et al., 1995), whereas the proportion of large copepods and krill in the diet of juvenile pollock increased with increasing fish size (Schabetsberger et al., 2000). In another study, adult walleye pollock fed on decapods and krill in higher proportions than expected based on prey abundances (Brodeur, 1998). Although our results strongly suggest that the limitations of suction-induced flow fields contribute to the observed low proportions of evasive prey in larval fish guts, other mechanisms such as vision, prey size and armor, are also known to affect prey selectivity.

Flow patterns: comparison with previous studies
Previous experimental investigations into patterns of suction flows using particle image velocimetry (PIV) conformed to inviscid

models, such as that of Müller et al. (Müller et al., 1982). These studies showed a consistent spatial decay of flow speeds in front of the mouth and stereotypical temporal variation in flow speed as a function of the gape cycle (Day et al., 2005; Higham et al., 2006; Holzman et al., 2008a; Staab et al., 2012). Our simulations generated similar patterns to reported observations on fish with mouth diameters >3 mm. However, data for smaller fish are sparse, and extrapolations to flow properties in larval fish are thus difficult to make. The limited experimental data that do exist suggest that particles are captured from a distance greater than one mouth diameter (Hernández, 2000), consistent with our findings. Note that peak flow speeds obtained by our model were around twice the PIV measurements recorded for other species with similar-sized mouths (Higham et al., 2006; Holzman et al., 2008a). This discrepancy in peak flow speeds could be due to inter-species differences in mouth volume and kinematics (PIV data not available for *S. aurata*) and to the fact that opercular opening was excluded from our simulations [as in other models (Müller et al., 1982; Van Wassenbergh and Aerts, 2009)].

Models of suction feeding often make the simplifying assumption of inviscid flow. Such treatment was recently justified for large fish (mouth diameter ~3.5 mm, $Re>10^4$), in which violations of this assumption have only a minimal effect on the spatial pattern of flow in front of the mouth (Van Wassenbergh and Aerts, 2009). Models that operate under this assumption have proved instrumental in predicting the spatial and temporal patterns of flow speed in front of the mouth, the distribution of suction pressure, the work required to expand the mouth cavity and the relationships between expansion kinematics and flow speed (Bishop et al., 2008; Müller et al., 1982; Van Wassenbergh et al., 2006a). However, for mouth diameters smaller than 0.5 mm, the inviscid model of Bishop et al. (Bishop et al., 2008) over-estimated peak flow speeds by 33–66% compared with the present model (Fig. 3C) and Re values calculated on the basis of CFD were two to three times larger than those estimated using the inviscid model (Fig. 1D). A separate model, which describes a circular vortex in front of the mouth and also assumes inviscid flow (Müller et al., 1982), was also found not to accord with our results at small mouth sizes. In mouths with small diameters (≤0.5 mm), the decay of flow speed was more gradual in our CFD model compared with the model of Müller et al. (Müller et al., 1982) (see Figs 3–5). These results contrast with the common notion that the decay of flow speed is a relatively invariant function of distance from the mouth (Day et al., 2005; Higham et al., 2006; Holzman et al., 2008a; Müller et al., 1982; Staab et al., 2012; Van Wassenbergh and Aerts, 2009).

A two-dimensional (2D) CFD model for suction-feeding carp larvae (peak gape diameter=0.256 mm) predicted that viscosity would have a strong effect on the energy required to open the mouth and reported a strong flow speed gradient across the aperture (Drost et al., 1988). The authors of that study did not report the marked

effects of size on flow pattern that we obtained here. It is, however, difficult to directly compare these findings with the present results because the earlier study employed a much coarser computational grid and assumed a more simplified model of two separating plates. This difference in modeled mouth shape can potentially strongly influence the inferred flow. For example, Bishop et al. reported that peak flow speed was three times higher when the expanding mouth was modeled as a single cone compared with a triple cone, even when mouth-opening time and peak volume were similar (Bishop et al., 2008). Moreover, the 2D CFD model (Drost et al., 1988) invoked a faster expansion time (8 ms) and produced flow speeds greater than $0.6\,\mathrm{m\,s^{-1}}$, which correspond to $Re>100$. In the present study, deviations from the inviscid models were most pronounced at $Re<100$. Although no experimental data are available on suction flow speeds in larval fish, flows of $0.6\,\mathrm{ms^{-1}}$ were measured for 60 mm juvenile bluegill sunfish (Holzman et al., 2008a) and could, therefore, be an over-estimation for a 6.5 mm larvae.

In summary, we developed an axi-symmetric computational model of mouth expansion that allows simulation of suction-induced flow fields across a large range of mouth sizes. The model is based on the observed isometric scaling of feeding morphology and independence of mouth opening speed with respect to body size in *Sparus auratus* (Fig. 1). The spatial pattern of suction flows changed dramatically during ontogeny, following the transition from low to high *Re* regimes. These changes have a strong effect on the forces exerted on prey and, consequently, on the nature of predator–prey interactions. The present results demonstrate that understanding the hydrodynamic properties of suction flow could be key to understanding larval feeding performance, which has direct consequences for larval starvation and mortality.

MATERIALS AND METHODS
Scaling of mouth cavity dimensions

We developed an axi-symmetric model of mouth cavity expansion, parameterized by empirical measurements of mouth cavity dimensions in *S. aurata* ranging in life stages from first feeding to adulthood. The model was composed of three compartments of constant axial lengths, L_1, L_2 and L_3 (Fig. 9A). These compartments represented the region from the mouth opening to the anterior hyoid (L_1), the region spanning the anterior to posterior length of the hyoid (L_2) and the region posterior to the hyoid extending to the opening of the esophagus (L_3). Mouth cavity expansion was simulated as time-dependent changes in the radii R_1, R_2 and R_3 of each compartment (as described in Eqn 1) in order to simulate an anterior-to-posterior wave of mouth opening (Fig. 9B) (Bishop et al., 2008). The radius R_1 represents the radius of the mouth aperture, referred to throughout the text as 'gape'. Thus, gape diameter equals $2\times R_1$. The radius R_4 at the esophagus opening was held constant throughout the simulation of mouth opening. The lengths B_1, B_2 and B_3 of the lateral surfaces of each compartment varied with time to fit the length variations of the radii R_1, R_2 and R_3. This is justified because the mouth walls (represented by the lateral surfaces of the compartments) are composed of flexible tissue that is attached to the skeleton. We simulated mouth expansion for seven mouth cavity lengths ($L=L_1+L_2+L_3$) of $L=0.25, 0.5, 1, 2, 5, 8$ and 40 mm.

Mouth cavity length L and peak gape diameter ($2\times R_{1,max}$) were measured for 67 *Sparus auratus* (gilt-head seabream). Fish spanned the ages of 5 to 180 days post hatching, and their total lengths ranged from 3.9 to 97 mm. Measurements were acquired using a calliper (resolution ±0.1 mm) for fish longer than 35 mm and under a dissecting microscope for smaller fish. The measured values of peak gape diameter and mouth cavity length ranged from 0.09–6 mm and 0.5–53 mm, respectively. The scaling of peak gape diameter with respect to mouth cavity length was close to a slope of 1 (see Results). Internal dimensions of R_2, R_3, L_1, L_2 and L_3 were measured from a silicone cast of the maximally open mouth of a *S. aurata* sub-adult (5 cm, total length). The cast was constructed by injecting commercial silicon sealant into the mouths of freshly killed fish and dissecting out the cast after
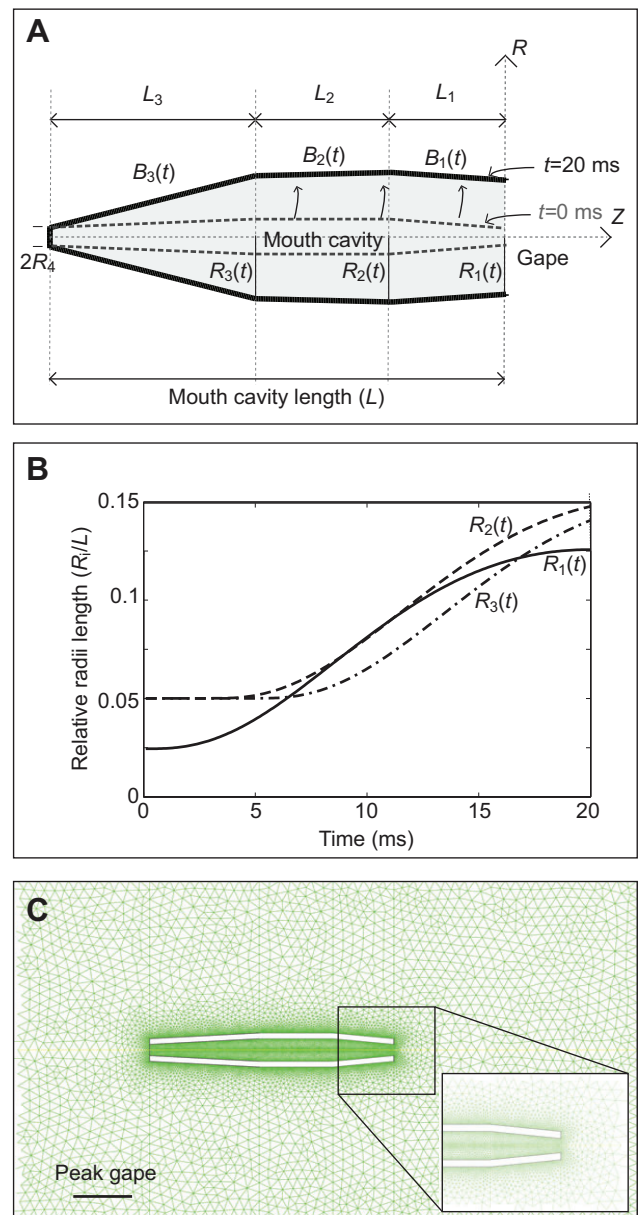
Fig. 9. Mouth cavity geometry, opening kinematics and mesh design. (A) A schematic description of the model cross-section at $t=0$ ms (dotted gray lines) and at peak volume expansion ($t=20$ ms; solid black lines). The length L of the axi-symmetric model was divided into three segments (L_1–L_3) whose lengths were fixed with respect to time, whereas the length (B_1–B_3) of lateral surfaces of each compartment increased when the mouth opened. R_4 was designated as the back wall of the model and was fixed with respect to time. The model was also fixed with respect to the longitudinal axis, with the center of the mouth aperture located at the origin [$(R,Z)=(0,0)$]. The shaded area represents a frontal section of the mouth cavity at $t=20$ ms. The radii R_1–R_3 were time-dependent (Eqn 1; B). (B) Mouth cavity opening. Lines represent the change in mouth radii R_1, R_2 and R_3 with time (t). (C) Mesh design around and within mouth cavity model ($2\times R_{1,max}=10$ mm) inside the 3D tank before expansion ($t=0$ ms). The inset shows the details of the mouth aperture. The yellow line denotes the symmetry axis. The scale bar is equivalent to peak gape diameter.

it had cured. Measurements were acquired from anatomical landmarks (e.g. mouth aperture, hyoid, esophagus) impressed in the cured silicon cast. On the basis of these measurements, we set L_1, L_2 and L_3 as 25%, 30% and 45% of mouth cavity length L and the maximal radii of R_1, R_2 and R_3 was set to 12.5%, 15% and 15% of mouth cavity length, respectively (Fig. 9A,

Table 1. Parameters defining mouth cavity geometry and expansion (Eqn 1)

Parameter	L=40 mm	L=8 mm	L=5 mm	L=2 mm	L=1 mm	L=0.5 mm	L=0.25 mm
$R_1(t=0)$	2	0.4	0.25	0.1	0.05	0.025	0.0125
$R_2(t=0)$, $R_3(t=0)$	4	0.8	0.5	0.2	0.1	0.05	0.025
$R_1(t=20)$, $R_2(t=20)$, $R_3(t=20)$	10	2	1.25	0.5	0.25	0.125	0.0625
L_1	10	2	1.25	0.5	0.25	0.125	0.0625
L_2	12	2.4	1.5	0.6	0.3	0.15	0.075
L_3	18	3.6	2.25	0.9	0.45	0.225	0.1125

t_0 of R_1= 0 ms; t_0 of R_2=3 ms; t_0 of R_3=5 ms; t_{max} of R=20 ms; t_{max} of R_2=23 ms; t_{max} of R_3=25 ms.

Table 1). Following Bishop et al. (Bishop et al., 2008), mouth radii R_1, R_2 and R_3 at rest (before mouth expansion) were set to 2.5%, 5% and 5% of mouth cavity length, respectively.

Scaling of mouth cavity expansion
The pattern of mouth opening was simulated by varying the radii $R(t)$ of each mouth section (R_1, R_2 and R_3) using the following time-dependent exponential function (Müller et al., 1982):

$$R(t) = R_0 + R_{max}\left[\frac{(t-t_0)}{t_{max}}\exp\left(1-\frac{t_0-t}{t_{max}}\right)\right]^2. \tag{1}$$

Here, R_0=$R(t=0)$, namely the initial R. t_0 is the time when R first deviates from R_0 and t_{max} is the time when R is maximal (R=R_{max}; Fig. 9B). Note that the radius of each mouth section can have different R_0, t_0, R_{max} and t_{max} values (Table 1).

We used high-speed video to characterize *S. aurata* mouth expansion. Larvae at 7–65 days post hatching were filmed in a small filming chamber (70×30×10 mm) while feeding on rotifers (*Brachionus rotundiformis*; ~80 μm in length) and *Artemia* nauplii (24–48 h post hatching; ~250 μm in length). A continuous high-speed recording system (Vieworks VC-4MC-M/C 180 high speed CMOS camera) equipped with a 25 mm c-mount macro lens (Avenir CCTV lens, Seikou Optical Ltd, Tokyo, Japan) was employed to record 20-min-long sequences of larval feeding. Filming was conducted at 500 frames per second, with a resolution of 2048×800 pixels. We randomly selected two or three sequences from each age group for analysis (7, 9, 12, 15, 18, 22, 25, 29, 35, 42, 65 days post hatching). Post-larval fish (standard length 35–100 mm) were filmed as described previously (Oufiero et al., 2012), except that the camera used here was a Photron SA6 (Photron, Japan). These fish were fed commercial flakes and fish meat. One sequence was selected for analysis for each of 18 large individuals filmed. All feeding trials described above complied with IACUC-approved guidelines for the use and care of animals in research at Tel Aviv University, Israel.

For each sequence, we tracked external landmarks across frames to determine peak gape diameter and the time to peak gape [defined as the time it took the mouth to open from 20% to 95% of maximal diameter (Oufiero et al., 2012)]. In addition, we digitized the location of the prey and the mouth at t=0 ms (the time when the mouth started opening) for 40 strikes in which the prey was clearly visible at that time (i.e. not obscured by other fish or outside the frame). From these data, we calculated the distance (in units of peak gape diameter) and angle (relative to the longitudinal axis of the body) between the prey and mouth center.

Because the time to peak gape (a proxy for mouth-opening speed) showed no relationship with changing mouth cavity length (see Results), the temporal pattern of mouth opening was held constant for all our models, across the range of peak gape values. The anterior section of the mouth opened first, reaching peak gape diameter (2×$R_{1,max}$) at t=20 ms. The timing of expansion of R_2 and R_3 was based on the parameters obtained by Bishop et al. (Bishop et al., 2008), with the anterior section starting to open at t=3 ms and reaching $R_{2,max}$ at t=23 ms. Expansion of the posterior section was delayed 2 ms after that of the central section (Fig. 9B; Table 1). In fish, the anterior-to-posterior wave of expansion ends with the opening of the opercular slits. The present model did not include such openings and, hence, mouth-opening simulations were conducted until peak mouth expansion at t=20 ms (Bishop et al., 2008; Müller et al., 1982; Van Wassenbergh et al., 2006b).

Governing equations and computational approach
The mouth cavity model was immersed in a large fluid-filled rectangular domain. It was assumed that the inlet of the mouth cavity was open and, accordingly, fluid could flow in or out of the mouth. The flow field due to expansion of the mouth cavity model was governed by the continuity and momentum conservation equations for incompressible viscous laminar fluid flow in the absence of body force (Ferziger and Peric, 2001). Hence:

$$\frac{\partial \rho}{\partial t} + \nabla \cdot \rho \mathbf{V} = 0, \tag{2}$$

$$\frac{\partial \mathbf{V}}{\partial t} + \mathbf{V} \cdot \nabla \mathbf{V} = -\frac{1}{\rho}\nabla p + \frac{\mu}{\rho}\nabla^2 \mathbf{V}, \tag{3}$$

where $\mathbf{V}$ is the velocity vector, p is the pressure, ρ and μ are the density and dynamic viscosity of the fluid, respectively. Note that the first term in Eqn 2 is zero for an incompressible fluid.

The boundary conditions of no slip and no penetration were applied along interfaces between the fluid and the walls of the mouth cavity model. The flow field was induced by movement of the mouth walls as dictated by mouth opening (Eqn 1). The governing equations of the present model (Eqns 1–3) were solved using the finite volume FLUENT computational package (Ansys, Lebanon, NH). The axi-symmetric expansion of the mouth walls was implemented via a subroutine in the computational code as determined by Eqn 1. The geometry of the fluid domain was converted into a discrete mesh using Workbench (Ansys). A mesh of triangular cells was defined with mesh points more clustered around the mouth walls, where steep gradients of flow speed were expected (Fig. 9C). The number of elements for the present simulation was chosen to be 20,000 with 20,000 time-steps of 10^{-6} s. Mesh validation was performed by comparing axial flow speed profiles at two cross-sections (along the mouth center line and the mouth outlet) for two different mesh densities (20,000 and 80,000 cells) at t=10 ms and t=20 ms. The difference in maximal velocities on the two cross sections in the two meshes was less than 1% in the two time periods. Therefore, the mesh of 20,000 cells was chosen for study.

The segregated iterative method was used to obtain non-linear solutions at each time step of the non-linear time-dependent problem with the selected implicit time integration scheme. The complete numerical solution was obtained by imposing a convergence criterion of 10^{-3} for the continuity and flow speed components. To ensure that this convergence criterion was sufficiently low to enable prediction of results, it was verified that the model conserves mass. The right wall of the rectangular container in which the mouth was submerged (the 'aquarium' containing the mouth), was defined as an outlet. If the model failed to converge, mass would be added or removed from the computational domain and fluid would flow in and out of that outlet. The integral of the flow rate over time was calculated for the duration of the simulation at the domain wall. The total flow through this surface was zero, indicating conservation of mass.

For each model size, we also calculated the Reynolds number (Re) at the center of the mouth, based on gape diameter [$2×R_1(t)$] as the characteristic length and flow speed at the center of the mouth aperture $U_m(t)$. Despite the high Re that occurred at specific regions and times (e.g. Re>10^4 on the center line around peak flow speed), it was assumed that flow was laminar in the model. Consequently, FLUENT neglected turbulence terms when solving Navier–Stokes equations as the transition to turbulence in accelerating flows is considerably delayed and occurs only above Re=2×10^5 (Greenblatt and Moss, 2003; Annus and Koppel, 2011).

Scaled variables and analysis of flow patterns

Flow characteristics that are potentially important in determining feeding performance were computed for each model. To study the flow pattern in front of the fish's mouth, we defined a cylindrical coordinate system with the origin at the mouth center and the longitudinal axis set parallel to the mouth center line (Fig. 2). In this coordinate system, the position of a point P can be described by the radial distance (R=the perpendicular distance from the longitudinal axis to the point P), the azimuth [φ=the angle between a reference direction on the chosen plane (i.e. the plane of the mouth) and the line from the origin to the projection of P on the plane], and the longitudinal distance (Z=the projected distance of p onto the longitudinal axis). Because the analysis is axi-symmetric, data are identical for all φ given the R,Z coordinates, hence, there is no need to reference φ.

The objective of this work was to explore differences in the flow pattern during suction-feeding in fish of different ages and body sizes. To enable comparison between the flow speeds for different mouth sizes, the distance variables and flow speeds were scaled to mouth diameter and maximum flow speed (at the mouth center), respectively, as in previous studies (Day et al., 2005; Day et al., 2007; Higham et al., 2006; Holzman et al., 2008a). The unit length for R and Z on the radial and longitudinal axes was defined as $2 \times R_{1,max}$, such that: $R=Z=d/(2 \times R_{1,max})$, where d is the Euclidean distance between the point P and the origin [$(R,Z)=(0,0)$]. Flow speed at any given point in time (t) and space (R,Z) is given as:

$$\upsilon(R,Z,t) = \frac{U(R,Z,t)}{U(R=0,Z=0,t=20)}, \qquad (4)$$

where $U(R=0,Z=0,t=20)$ is the flow speed at the center of the mouth aperture at time $t=20$ ms.

On this coordinate system, the flow speed parallel to the longitudinal axis was extracted at radial distances of $R=0$, 1/8, 1/4, 3/8 and 1/2. Flow speeds were extracted for $t=10$ and 20 ms. In previous work (Day et al., 2005; Van Wassenbergh and Aerts, 2009) and for the large mouths addressed here (see Results), Müller's inviscid model accurately described the decay of flow speed as a function of distance from the mouth. However, this model did not fit low Re cases (see Results). Therefore, for each radial distance two summary statistics were calculated namely, the scaled distance $Z_{1/2}$ at which flow speed was half its maximum value at the mouth [$\upsilon(R=0,Z,t)=\upsilon(R=0,Z=0,t)/2$], and the scaled distance $Z_{1/10}$ at which flow speed was one-tenth its maximum [$\upsilon(R=0,Z,t)=\upsilon(R=0,Z=0,t)/10$]. Patterns of flow speed on the above-mentioned transects were similar between time points ($t=10$ and 20 ms) and only results for $t=20$ ms are shown hereafter.

Capture of inert particles

The distance from which fish can capture inert prey was quantified by following the fate of inert particles in different mouth sizes. Trajectories of particles were computed from initial locations set outside the mouth on the cylindrical coordinate system. Particles were 1 μm in diameter and had a density of 1000 kg m^{-3}. Their spatial distribution at the time of mouth opening followed empirical data obtained from our high-speed videos (see supplementary material Fig. S1). Particles were distributed homogenously in front of the mouth such that the closest particle was located at [$(R,Z)=(0,0)$] and the furthest at [$(R,Z)=(0.78,1.5)$]. The distance between particles was $R=Z=0.06$. Overall, the trajectories of 364 particles were tracked until peak mouth expansion. The arrangement of the particles at $t=0$ ms is depicted in Fig. 2 and supplementary material Table S1. For each model, the proportion of particles entrained was calculated.

Capture of evasive prey

We used the suction-induced force-field model (SIFF; see below for details) to estimate forces exerted on actively swimming prey, given flow fields computed from our fluid flow model. Given user-specified parameter values to characterize the prey (e.g. size, escape thrust), the SIFF model simulates predator–prey encounters and predicts motion of the prey relative to the mouth during suction feeding (Holzman et al., 2007; Wainwright and Day, 2007). Here, the SIFF model was parameterized for each mouth size based on CFD results, measured morphology and strike kinematics of *S. aurata*, and we investigated the relationship between peak gape diameter, prey escape thrust and prey capture success. We note that CFD solvers can also

solve prey movements, but the required computation time is much longer than in SIFF (days as opposed to seconds), and the shortened time allowed us to run SIFF iteratively over varying prey escape forces (see below).

In this analysis, the prey was considered captured if it crossed the aperture into the mouth cavity. The forces were calculated for neutrally buoyant prey, which were initially located on the longitudinal axis in front of the mouth. Although the prey of larval and adult fish differ greatly in size, shape and sensory ability, these properties were held constant throughout the simulations so as to isolate the effect of hydrodynamics on prey-capture performance. Prey were elliptical, 80 μm long and 30 μm wide, similar to the dimensions of rotifers. Simulation with prey that had length and width of 1/4 and 1/8 of mouth diameter yielded similar patterns that did not change our interpretations (data not shown). Simulations excluded ram and jaw protrusion (i.e. no displacement of the mouth along the longitudinal axis). Prey responded to the approaching predator by exerting an escape force that initiated when flow speed exceeded a threshold of 0.013 m s^{-1}. The escaping prey thrust peaked after 10 ms, similar to the patterns produced by escaping copepods (Buskey et al., 2002). For each mouth size, we ran SIFF for 36 initial prey positions, equally spaced on the longitudinal axis from a distance of $Z=0.1$ to $Z=1.5$. For each prey, the simulation was initiated with a low escape force (1×10^{-30} N). If the prey was captured, the escape force increased by 50% and the simulation was re-run until the prey had escaped the predator. The prey escape force in the last simulation was recorded as an indication of the minimum force required for the prey to avoid capture at each starting position (which we refer to throughout as 'escape thrust').

The predicted values of the escape thrust needed to escape the suction flows produced by mouths with peak gape diameter >0.5 mm were in the range of 10^{-7} to 10^{-10} N, corresponding to accelerations of ~1000 to 1 m s^{-2} (see Results). These accelerations are in the observed range of accelerations in copepods, which are known to produce accelerations faster than 200 m s^{-2} (Buskey and Hartline, 2003; Kiørboe et al., 2009). In our simulations, the prey could escape mouths with peak gape diameter <0.5 mm by generating accelerations slower than 20 m s^{-2}.

A model of the forces exerted on the prey (SIFF)

The computed results of the flow field were used to estimate the forces exerted on prey, which can be simulated as an active particle within an unsteady flow field. This model uses the flow field realised during the strike and a set of parameters that characterize the prey and the mouth in order to predict the motion of prey relative to the mouth during suction-feeding (Holzman et al., 2007; Wainwright and Day, 2007). According to this SIFF model, the movement of the prey relative to the predator's mouth determines prey capture. The total force exerted on the prey is the sum of five component forces: drag, acceleration reaction force, the force resulting from the pressure gradient across the prey, prey swimming forces and gravitational forces [the latter will be ignored in the current discussion as most aquatic organisms are approximately neutrally buoyant (Wainwright and Day, 2007)]. These forces result from the differential in speeds and accelerations between the prey and the water around it, as well as from the gradient of flow across the prey (Wainwright and Day, 2007). Flow speed derivatives in front of the mouth are driven by the temporal pattern of flow at the mouth (flow speeds accelerating during the strike), changes in peak gape diameter and decay of flow speed with the distance from the mouth. In addition, if the prey does not move as a water particle (e.g. when escaping), differential flow speed and acceleration form between the prey and the fluid around it. These differentials are manifested in drag and acceleration reaction forces, respectively. The effects of flow on the prey are also mediated by properties of the prey itself, such as its size and length, as well as drag and added mass coefficients. These summarize small-scale interactions between the unsteady flow field and the solid object within it (Holzman et al., 2008b; Skorczewski et al., 2010; Wainwright and Day, 2007). In other words, the model assumes that all the fluid–structure interactions around the body of the prey are captured by the drag and added mass coefficients. We applied SIFF in order to determine these forces and sum them over small increments of time, solved the acceleration, speed and movement of the prey and used these in order to predict the strike outcome, namely prey capture or escape.

Supplementary material
Supplementary material available online at
http://jeb.biologists.org/lookup/suppl/doi:10.1242/jeb.104331/-/DC1

References
Annus, I. and Koppel, T. (2011). Transition to turbulence in accelerating pipe flow. *J. Fluids Eng.* **133**, 071202.

Anto, J. and Turingan, R. G. (2010). Relating the ontogeny of functional morphology and prey selection with larval mortality in *Amphiprion frenatus*. *J. Morphol.* **271**, 682-696.

Bishop, K. L., Wainwright, P. C. and Holzman, R. (2008). Anterior-to-posterior wave of buccal expansion in suction feeding fishes is critical for optimizing fluid flow velocity profile. *J. R. Soc. Interface* **5**, 1309-1316.

Brodeur, R. (1998). Prey selection by age-0 walleye pollock, *Theragra chalcogramma*, in nearshore waters of the Gulf of Alaska. *Environ. Biol. Fishes* **51**, 175-186.

Buskey, E. J. and Hartline, D. K. (2003). High-speed video analysis of the escape responses of the copepod *Acartia tonsa* to shadows. *Biol. Bull.* **204**, 28-37.

Buskey, E. J., Lenz, P. H. and Hartline, D. K. (2002). Escape behavior of planktonic copepods in response to hydrodynamic disturbances: high speed video analysis. *Mar. Ecol. Prog. Ser.* **235**, 135-146.

Checkley, D. (1982). Selective feeding by Atlantic herring (*Clupea harengus*) larvae on zooplankton in natural assemblages. *Mar. Ecol. Prog. Ser.* **9**, 245-253.

Chesson, J. (1983). The estimation and analysis of preference and its relationship to foraging models. *Ecology* **64**, 1297-1304.

China, V. and Holzman, R. (2014). Hydrodynamic starvation in first-feeding larval fishes. *Proc. Natl. Acad. Sci. USA* **111**, 8083-8088.

Cowen, R. (2002). Larval dispersal and retention and consequences for population connectivity. In *Coral Reef Fishes. Dynamics and Diversity in a Complex Ecosystem* (ed. P. F. Sale), pp. 149-170. San Diego, CA: Academic Press.

Danos, N. and Lauder, G. V. (2012). Challenging zebrafish escape responses by increasing water viscosity. *J. Exp. Biol.* **215**, 1854-1862.

Day, S. W., Higham, T. E., Cheer, A. Y. and Wainwright, P. C. (2005). Spatial and temporal patterns of water flow generated by suction-feeding bluegill sunfish *Lepomis macrochirus* resolved by Particle Image Velocimetry. *J. Exp. Biol.* **208**, 2661-2671.

Day, S. W., Higham, T. E. and Wainwright, P. C. (2007). Time resolved measurements of the flow generated by suction feeding fish. *Exp. Fluids* **43**, 713-724.

Drost, M. R. (1987). Relation between aiming and catch success in larval fishes. *Can. J. Fish. Aquat. Sci.* **44**, 304-315.

Drost, M. R., Müller, M. and Osse, J. W. M. (1988). A quantitative hydrodynamical model of suction feeding in larval fishes – the role of frictional forces. *Proc. R. Soc. B* **234**, 263-281.

Fernández-Diaz, C., Pascual, E. and Yúfera, M. (1994). Feeding behaviour and prey size selection of gilthead seabream, *Sparus aurata*, larvae fed on inert and live food. *Mar. Biol.* **118**, 323-328.

Ferziger, J. H. and Peric, M. (2001). *Computational Methods for Fluid Dynamics*. Berlin: Springer.

Fyhn, H. J. (1989). 1st feeding of marine fish larvae – are free amino-acids the source of energy? *Aquaculture* **80**, 111-120.

Greenblatt, D. and Moss, E. A. (2003). Rapid transition to turbulence in pipe flows accelerated from rest. *J. Fluids Eng.* **125**, 1072-1075.

Hernández, L. P. (2000). Intraspecific scaling of feeding mechanics in an ontogenetic series of zebrafish, *Danio rerio*. *J. Exp. Biol.* **203**, 3033-3043.

Higham, T. E., Day, S. W. and Wainwright, P. C. (2006). Multidimensional analysis of suction feeding performance in fishes: fluid speed, acceleration, strike accuracy and the ingested volume of water. *J. Exp. Biol.* **209**, 2713-2725.

Hillgruber, N., Haldorson, L. and Paul, A. (1995). Feeding selectivity of larval walleye pollock *Theragra chalcogramma* in the oceanic domain of the Bering Sea. *Mar. Ecol. Prog. Ser.* **120**, 1-10.

Holzman, R. and Genin, A. (2003). Zooplanktivory by a nocturnal coral-reef fish: effects of light, flow, and prey density. *Limnol. Oceanogr.* **48**, 1367-1375.

Holzman, R., Day, S. W. and Wainwright, P. C. (2007). Timing is everything: coordination of strike kinematics affects the force exerted by suction feeding fish on attached prey. *J. Exp. Biol.* **210**, 3328-3336.

Holzman, R., Collar, D. C., Day, S. W., Bishop, K. L. and Wainwright, P. C. (2008a). Scaling of suction-induced flows in bluegill: morphological and kinematic predictors for the ontogeny of feeding performance. *J. Exp. Biol.* **211**, 2658-2668.

Holzman, R., Day, S. W., Mehta, R. S. and Wainwright, P. C. (2008b). Jaw protrusion enhances forces exerted on prey by suction feeding fishes. *J. R. Soc. Interface* **5**, 1445-1457.

Holzman, R., Collar, D. C., Mehta, R. S. and Wainwright, P. C. (2012). An integrative modeling approach to elucidate suction-feeding performance. *J. Exp. Biol.* **215**, 1-13.

Houde, E. D. and Schekter, R. C. (1980). Feeding by marine fish larvae – developmental and functional responses. *Environ. Biol. Fishes* **5**, 315-334.

Hunter, R. J. (1980). The feeding behavior and ecology of marine fish larvae. In *ICLARM Conference Proceedings* **5**, 287-330.

Hunter, J. P. (1981). Feeding ecology and predation of marine fish larvae. In *Marine Fish Larvae: Morphology, Ecology, and Relation to Fisheries*, pp. 33-77 (ed. R. Lasker). Seattle, WA: University of Washington Press.

Kane, E. A. and Higham, T. E. (2014). Modelled three-dimensional suction accuracy predicts prey capture success in three species of centrarchid fishes. *J. R. Soc. Interface* **11**, 20140223.

Kent, R., Holzman, R. and Genin, A. (2006). Preliminary evidence on group-size dependent feeding success in the damselfish Dascyllus marginatus. *Mar. Ecol. Prog. Ser.* **323**, 299-303.

Kiørboe, T., Andersen, A., Langlois, V. J., Jakobsen, H. H. and Bohr, T. (2009). Mechanisms and feasibility of prey capture in ambush-feeding zooplankton. *Proc. Natl. Acad. Sci. USA* **106**, 12394-12399.

Leis, J. and McCormick, M. (2002). The biology, behavior, and ecology of the pelagic, larval stage of coral reef fishes. In *Coral Reef Fishes. Dynamics and Diversity in a Complex Ecosystem* (ed. P. F. Sale), pp. 171-199. San Diego, CA: Academic Press.

Müller, U. K. and van Leeuwen, J. L. (2004). Swimming of larval zebrafish: ontogeny of body waves and implications for locomotory development. *J. Exp. Biol.* **207**, 853-868.

Müller, U. K. and Videler, J. J. (1996). Inertia as a 'safe harbour': do fish larvae increase length growth to escape viscous drag? *Rev. Fish Biol. Fish.* **6**, 353-360.

Müller, M., Osse, J. W. M. and Verhagen, J. H. G. (1982). A quantitative hydrodynamical model of suction feeding in fish. *J. Theor. Biol.* **95**, 49-79.

Müller, U. K., van den Boogaart, J. G. M. and van Leeuwen, J. L. (2008). Flow patterns of larval fish: undulatory swimming in the intermediate flow regime. *J. Exp. Biol.* **211**, 196-205.

Osse, J. W. M. (1989). Form changes in fish larvae in relation to changing demands of function. *Neth. J. Zool.* **40**, 362-385.

Osse, J. and van den Boogaart, J. G. M. (1999). Dynamic morphology of fish larvae, structural implications of friction forces in swimming, feeding and ventilation. *J. Fish Biol.* **55**, 156-174.

Oufiero, C. E., Holzman, R. A., Young, F. A. and Wainwright, P. C. (2012). New insights from serranid fishes on the role of trade-offs in suction-feeding diversification. *J. Exp. Biol.* **215**, 3845-3855.

Robert, D., Levesque, K., Gagné, J. A. and Fortier, L. (2011). Change in prey selectivity during the larval life of Atlantic cod in the southern Gulf of St Lawrence. *J. Plankton Res.* **33**, 195-200.

Schabetsberger, R., Brodeur, R. D., Ciannelli, L., Napp, J. M. and Swartzman, G. L. (2000). Diel vertical migration and interaction of zooplankton and juvenile walleye pollock (*Theragra chalcogramma*) at a frontal region near the Pribilof Islands, Bering Sea. *ICES J. Mar. Sci.* **57**, 1283-1295.

Skorczewski, T., Cheer, A., Cheung, S. and Wainwright, P. C. (2010). Use of computational fluid dynamics to study forces exerted on prey by aquatic suction feeders. *J. R. Soc. Interface* **7**, 475-484.

Sponaugle, S., Walter, K. D., Denit, K. L., Llopiz, J. K. and Cowen, R. K. (2010). Variation in pelagic larval growth of Atlantic billfishes: the role of prey composition and selective mortality. *Mar. Biol.* **157**, 839-849.

Staab, K. L., Holzman, R., Hernandez, L. P. and Wainwright, P. C. (2012). Independently evolved upper jaw protrusion mechanisms show convergent hydrodynamic function in teleost fishes. *J. Exp. Biol.* **215**, 1456-1463.

Stoecker, D. K. and Govoni, J. J. (1984). Food selection by young larval gulf menhaden (Brevoortia patronus). *Mar. Biol.* **80**, 299-306.

Tancioni, L., Mariani, S., Maccaroni, A., Mariani, A., Massa, F., Scardi, M. and Cataudella, S. (2003). Locality-specific variation in the feeding of *Sparus aurata* L.: evidence from two Mediterranean lagoon systems. *Estuar. Coast. Shelf Sci.* **57**, 469-474.

Tuck, E. O. (1970). Unsteady flow of a viscous fluid from a source in a wall. *J. Fluid Mech.* **41**, 641-652.

Van Wassenbergh, S. and Aerts, P. (2009). Aquatic suction feeding dynamics: insights from computational modelling. *J. R. Soc. Interface* **6**, 149-158.

Van Wassenbergh, S., Aerts, P. and Herrel, A. (2006a). Hydrodynamic modelling of aquatic suction performance and intra-oral pressures: limitations for comparative studies. *J. R. Soc. Interface* **3**, 507-514.

Van Wassenbergh, S., Aerts, P. and Herrel, A. (2006b). Scaling of suction feeding performance in the catfish Clarias gariepinus. *Physiol. Biochem. Zool.* **79**, 43-56.

Wainwright, P. C. and Day, S. W. (2007). The forces exerted by aquatic suction feeders on their prey. *J. R. Soc. Interface* **4**, 553-560.

Wainwright, P., Carroll, A. M., Collar, D. C., Day, S. W., Higham, T. E. and Holzman, R. A. (2007). Suction feeding mechanics, performance, and diversity in fishes. *Integr. Comp. Biol.* **47**, 96-106.